

$\alpha_v\beta_3$ Integrin-Targeted PLGA-PEG Nanoparticles for Enhanced Anti-tumor Efficacy of a Pt(IV) Prodrug

Nora Graf,[†] Diane R. Bielenberg,[‡] Nagesh Kolishetti,[§] Christoph Muus,[†] Jacqueline Banyard,[‡] Omid C. Farokhzad,[§] and Stephen J. Lippard^{†,*}

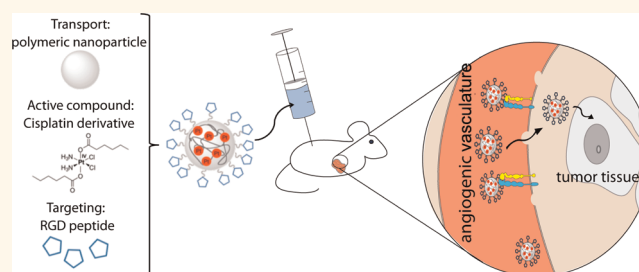
[†]Department of Chemistry, Massachusetts Institute of Technology, Cambridge, Massachusetts 02139, United States, [‡]Children's Hospital and Harvard Medical School, Vascular Biology Program, Boston, Massachusetts 02115, United States, and [§]Laboratory of Nanomedicine and Biomaterials, Department of Anesthesiology, Brigham and Women's Hospital and Harvard Medical School, Boston, Massachusetts 02115, United States

Cisplatin is one of the most widely used anticancer drugs most notably for the treatment of ovarian and testicular cancer. Current research focuses on minimizing side effects like liver and kidney toxicity and overcoming resistance of the drug while maintaining its potency against cancer cells, thereby extending successful treatment to a wider range of human cancers.¹ For example, as a single agent, cisplatin can only achieve up to 10% response rates in pre-treated breast cancer patients.²

Only 5–10% of the Pt(II) compound cisplatin that enters cells binds to nuclear DNA, the target responsible for its anticancer activity; the remainder is associated with proteins and low molecular weight biomolecules.³ It is therefore important to deliver as much of the injected platinum as possible to the cancer cell. A promising strategy for achieving this goal is to employ Pt(IV) complexes as prodrugs that can be intracellularly activated by reduction to generate Pt(II).⁴ The greater kinetic inertness of Pt(IV) compared to more labile Pt(II) complexes has the potential to enable a larger amount of drug to arrive at the tumor site intact by avoiding side reactions with proteins and other biomolecules in the process. Thus Pt(IV) compounds in general are expected to be less toxic and produce fewer side effects *in vivo*. Pt(IV) complexes accumulated in the hypoxic tumor environment become reduced to more reactive Pt(II) analogues.⁵

For increasing drug efficacy, targeted delivery to cancer cells is desirable.⁶ This selectivity can be achieved by exploiting the presence of proteins upregulated in cancer cells. Among these are integrins, heterodimeric cell adhesion proteins that have been linked to both tumor angiogenesis and

ABSTRACT



Targeted delivery of therapeutics to tumor neovasculature is potentially a powerful approach for selective cancer treatment. Integrins are heterodimeric transmembrane proteins involved in cell adhesion and cell signaling, and their expression is commonly upregulated in cancers and inflammatory diseases. The $\alpha_v\beta_3$ integrin is differentially upregulated on angiogenic endothelial cells as well as on many cancer cells. Here we demonstrate the differential targeting of cisplatin prodrug-encapsulated poly(D,L-lactic-co-glycolic acid)-block-polyethylene glycol (PLGA-PEG) nanoparticles (NPs) to the $\alpha_v\beta_3$ integrin on cancer cells using the cyclic pentapeptide c(RGDfK). Cisplatin is one of the most widely used anticancer drugs, and approaches that can improve its therapeutic index are of broad importance. The RGD-targeted Pt(IV)-encapsulated NPs displayed enhanced cytotoxicity as compared to cisplatin administered in its conventional dosage form in model prostate and breast cancer epithelial cells *in vitro*. Cytotoxicities were also elevated in comparison to those of previously reported systems, a small molecule Pt(IV)-RGD conjugate and a Pt(IV) nanoscale coordination polymer carrying RGD moieties. This result encouraged us also to evaluate the anticancer effect of the new construct in an animal model. The RGD-targeted PLGA-PEG NPs were more efficacious and better tolerated by comparison to cisplatin in an orthotopic human breast cancer xenograft model *in vivo*.

KEYWORDS: RGD peptide · integrin targeting · Pt(IV) complex · polymeric nanoparticle · breast cancer xenograft

metastasis.^{7,8} The integrin receptor is highly upregulated in tumor-associated endothelial cells during angiogenesis in a wide range of fast growing tumors in contrast to its minimal expression in quiescent endothelial cells in most normal tissues.⁹ Targeting the tumor vasculature is a powerful approach for cancer treatment because angiogenesis is essential for tumor growth

* Address correspondence to lippard@mit.edu.

Received for review March 15, 2012 and accepted April 24, 2012.

Published online May 14, 2012
10.1021/nn301148e

© 2012 American Chemical Society

and the vasculature is in direct contact with the bloodstream.¹⁰ A prominent example of a tumor vasculature-homing peptide is the three amino acid sequence RGD motif (arginine-glycine-aspartic acid).¹¹ RGD motifs are present in many extracellular matrix components such as fibronectin and vitronectin and bind to integrins on the cell surface. RGD analogues are used for tumor imaging and targeting with chemotherapeutic drugs or radionuclides. For example, a conjugate of the anticancer drug doxorubicin with RGD showed improved inhibition of breast tumor growth and metastatic dissemination in mice.¹⁰ Radiolabeled RGD peptides were targeted to xenograft tumors expressing $\alpha_v\beta_3$ integrins.^{12–14} With [¹⁸F]-galacto-RGD, the first RGD-based imaging agent was recently tested in humans, where it displayed highly desirable pharmacokinetics and good imaging of $\alpha_v\beta_3$ expression by PET.¹⁵ Previously, our group described the synthesis and biological evaluation of mono- and bifunctional Pt(IV)–peptide complexes containing RGD sequences as tumor-homing devices. Owing to selective binding to tumor cells, they were expected to be more effective than cisplatin, but none was able to exceed the efficacy of cisplatin.¹⁶

There is an increasing interest in nanocarriers such as inorganic and polymeric nanoparticles, nanotubes, nanophosphors, liposomes, and quantum dots coated with RGD analogues as targeting and imaging agents.^{17–24} Because polymeric nanoparticles are promising carriers for anticancer agents with significantly improved drug selectivity and controlled release,²⁵ we were motivated to investigate RGD-modified polymeric nanoparticles as cisplatin delivery vehicles. Nanocarriers with RGD ligands for the delivery of drugs have many advantages.²⁶ More drug molecules can be delivered per internalizing receptor, and the carriers are more likely to be internalized *via* receptor-mediated endocytosis than single RGD constructs owing to higher local ligand concentration and receptor cross-linking.^{26,27} The physicochemical properties of nanocarriers including their size, charge, porosity, surface hydrophilicity, and rigidity impact their pharmacokinetic and biodistribution properties *in vivo*. Optimization of these properties can result in the accumulation of nanocarriers in tumor tissue *via* the enhanced permeability and retention (EPR) phenomenon.²⁸ EPR is mediated by the leaky neovasculature, which is characteristic of tumors, resulting in nanocarrier extravasation into tumor interstitium and in the presence of poorly functioning lymphatic system in the tumors resulting in prolonged nanocarrier retention.

Improving the delivery of platinum-based anticancer agents by encapsulation in nanoparticles may lead to reduced side effects and achieve greater efficacy at lower doses.²⁹ Despite the advantages of nanocarriers to improve the safety and efficacy of cytotoxic drugs, there have been no such technologies clinically

approved for platinum chemotherapeutics. Examples in development and clinical trials include platinum–polymer complexes (*e.g.*, ProLindac), apoferritin, liposomes (*e.g.*, LipoPlatin), dendrimers, and micelles.^{30–32}

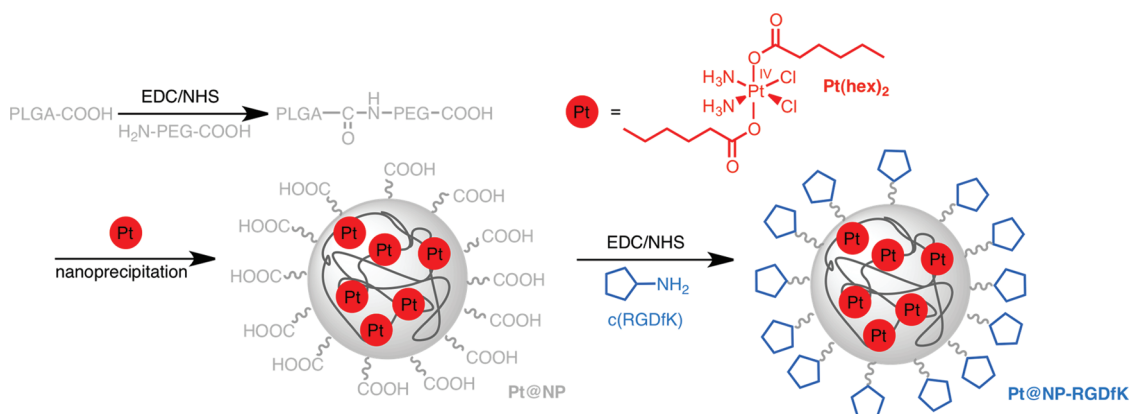
In order to circumvent pathways that deactivate a platinum-based drug by premature metabolism and protect non-cancerous cells from its effects, more inert Pt(IV) complexes can be used as redox-activatable prodrugs for Pt(II). Pt(IV) nanoconstructs, such as acid-responsive polymer–Pt(IV) conjugates³³ and nanoscale coordination polymers (NCPs) with RGD-targeting ligands,³⁴ have been reported. The former system showed increased cytotoxicity in comparison to cisplatin, whereas the latter did not.

Polymeric NPs have been used as a preferred nanoscale drug delivery vehicle especially for their excellent endocytosis, passive tumor-targeting, high encapsulation efficiency, and high stability, allowing for extended time in the circulatory system.³⁵ Noteworthy in this regard are controlled-release polymeric NPs based on clinically validated biodegradable poly(D,L-lactic-co-glycolic acid) (PLGA) polyesters with the degradation products being lactic acid and glycolic acid, which are naturally occurring substances that further break down into water and carbon dioxide.

Since the encapsulation of cisplatin into the hydrophobic polymeric nanoparticles is relatively inefficient, resulting in poor drug loading, we developed a strategy that significantly improves the encapsulation efficiency and drug loading of cisplatin in biodegradable nanoparticles of PLGA-*block*-polyethylene glycol (PLGA-PEG). As recently reported, a hydrophobic Pt(IV) compound was encapsulated in polymeric NPs and targeted to the prostate-specific membrane antigen (PSMA) expressing cells *in vitro* and *in vivo* using 2'-fluoropyrimidine-modified RNA aptamers that specifically bound the extracellular domain of PSMA.^{29,36,37} Here, we describe the synthesis and characterization of a polymeric NP construct that encapsulates a Pt(IV) complex in the core and is targeted to $\alpha_v\beta_3$ integrin-expressing cells using the cyclic pentapeptide c(RGDfK). We further report the *in vitro* cytotoxicity against several breast and prostate cancer cells and the evaluation of their $\alpha_v\beta_3$ integrin expression levels, as well as the *in vivo* efficacy of the construct in a breast cancer xenograft model. In this work, we thereby combine the approaches of active targeting of cell antigens and passive targeting by EPR, resulting in enhanced anti-tumor efficacy and reduced toxicity to normal tissues, the overall effect of which is a higher therapeutic index.

RESULTS AND DISCUSSION

Synthesis of c(RGDfK)-Functionalized Nanoparticles with Encapsulated Pt(IV) (Pt@NP-RGDfK). A hydrophobic Pt(IV) analogue of cisplatin, *c,c,t*-[PtCl₂(NH₃)₂(OOCCH₂CH₂CH₂CH₂CH₃)₂][Pt(hex)₂] (hex = hexanoato), was encapsulated



Scheme 1. Nanoprecipitation for generating Pt(IV)-encapsulated nanoparticles (Pt@NP) and functionalization with c(RGDfK) (Pt@NP-RGDfK). EDC = 1-ethyl-3-[3-dimethylaminopropyl]carbodiimide hydrochloride, NHS = *N*-hydroxysuccinimide.

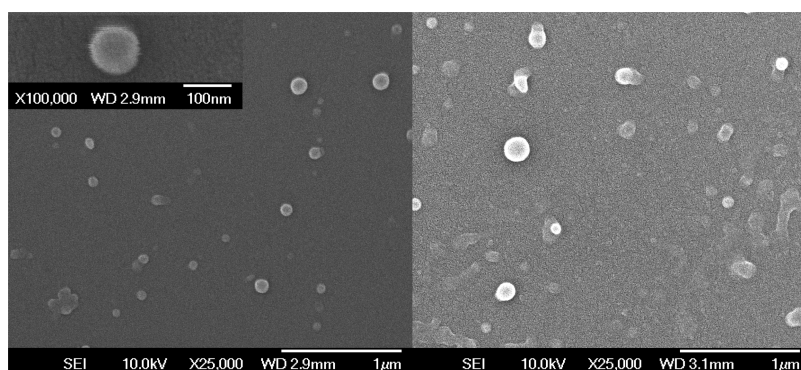


Figure 1. SEM images of PLGA-PEG nanoparticles with encapsulated Pt(hex)₂, unfunctionalized (left) and c(RGDfK)-functionalized (right). Magnification 25 000 \times , for inset 100 000 \times , voltage 10 kV.

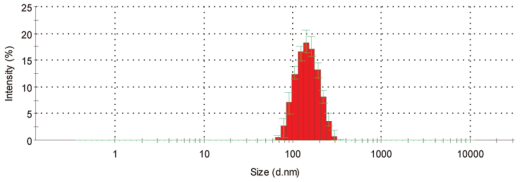
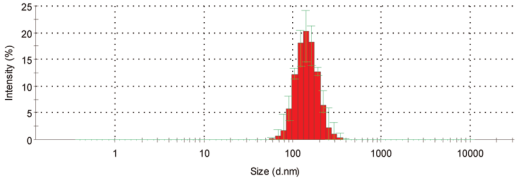
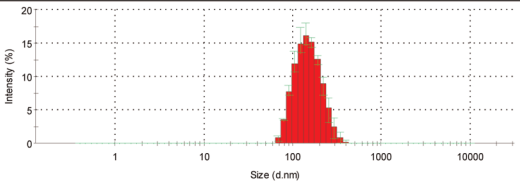
in PLGA-PEG NPs by nanoprecipitation (Pt@NP, Scheme 1).^{36,37} Whereas PLGA builds up the platinum-containing hydrophobic core, the hydrophilic PEG forms the corona to make carboxyl groups available for surface chemistry and provides steric stabilization and stealth properties against protein absorption and macrophage uptake,^{38,39} thus increasing NP circulation time. The success of the nanoprecipitation method was monitored by measuring the sizes and the polydispersity indices (PDI) of the NPs by dynamic light scattering (DLS). The sizes ranged from 75 to 140 nm, and PDIs were between 0.05 and 0.22 for all samples tested. The Pt content was measured by atomic absorption spectroscopy (AAS). Drug loading in over 20 independent experiments with different batches of polymer and 30–50% drug feed gave up to 1% loading, corresponding a maximum encapsulation efficiency of 3%. Alternatively, NPs were synthesized with a dispersing tool, resulting in particles of comparable sizes and PDIs to those formed by nanoprecipitation, exhibiting similar encapsulation efficiencies. To determine whether there was loss of polymeric material during synthesis, filtration, washing, and centrifugal concentration, one representative NP suspension batch was lyophilized and the polymeric residue weighed. Because 90% of the polymeric material was

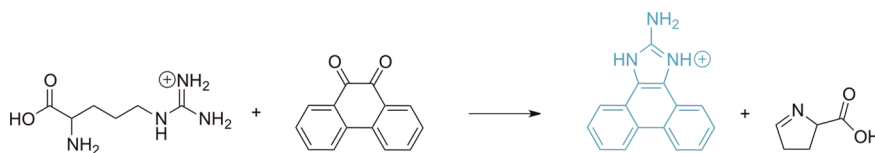
recovered with respect to the starting material, drug loading and encapsulation efficiencies referred to those of the starting material should be considered to have an error of 10%.

In the second step, the cyclic pentapeptide c(RGDfK) was coupled to the terminal carboxyl groups of the PEG moiety in Pt@NP (Scheme 1). The resulting Pt@NP-RGDfK was used to develop NPs for active targeting of $\alpha_v\beta_3$ integrin on cancerous cells and tumor neovasculature. The cyclization of the pentapeptide improves the binding properties; c(RGDfK) is one of the most effective artificial RGD peptides for targeting $\alpha_v\beta_3$.⁴⁰ For comparison of *in vitro* effects, we also synthesized a Pt-free analogue NP-RGDfK (*vide infra*).

The surface morphology and size of the nanoparticles Pt@NP and Pt@NP-RGDfK were determined by scanning electron microscopy (SEM). The SEM images (Figure 1) show NPs with diameters of approximately 100 nm, consistent with the results from DLS measurements. The images suggest that NPs begin to aggregate and form larger particles after functionalization. This process might be caused by the change in surface charge upon functionalization with the cyclic RGD peptide. On average, however, the NP size does not vary outside the experimental error range after functionalization (*cf.* Table 1).

TABLE 1. Characterization of Nanoparticles: Representative Size, PDI, and ζ Potential of Nanoparticles Formed by Nanoprecipitation with 40% Drug Feed before (Pt@NP) and after Functionalization with c(RGDfK) (Pt@NP-RGDfK) and NHS Ester Intermediate (Pt@NP-NHS)

	Size (nm)	Size distribution (intensity)	PDI	ζ potential (mV)
Pt@NP	138 \pm 5		0.07 \pm 0.01	-41.2 \pm 1.9
Pt@NP-NHS	139 \pm 2		0.05 \pm 0.05	-14.3 \pm 0.4
Pt@NP-RGDfK	141 \pm 5		0.12 \pm 0.03	-25.9 \pm 0.8



Scheme 2. Reaction of arginine with 9,10-phenanthrenequinone to yield a fluorescent product (blue).

The peptide content of Pt@NP-RGDfK was determined by measuring arginine using a previously described fluorimetric assay (Scheme 2 and Supporting Information Figure S1).⁴¹ The reagent 9,10-phenanthrenequinone was mixed with the sample at a high pH followed by acidification to convert arginine residues to a strongly fluorescent small molecule ($\lambda_{\text{ex}} = 312$, $\lambda_{\text{em}} = 340\text{--}570$ nm). Coupling reactions that were carried out with 1.1, 2, and 4% w/w c(RGDfK) with respect to the polymer all resulted in 1% w/w yield with respect to the polymer.

Qualitatively, the success of the peptide coupling was also checked by measuring the ζ potential of the NPs, which is the potential difference between the dispersion medium water and the stationary layer of fluid attached to the dispersed particle. All formulations exhibited a net negative charge with ζ potential values ranging from -41 to -14 mV depending on the nature of the functionalization (representative data are in Table 1). The data obtained for unfunctionalized NPs (Pt@NP) are similar to a literature reported value for PLGA-PEG nanoparticles of ~ 200 nm size having $\zeta = -31.4$ mV.²⁴ Functionalization of the NPs with c(RGDfK) (Pt@NP-RGDfK) led to no significant change

TABLE 2. Stability Tests with Pt Encapsulated in Nanoparticles of ~ 80 nm Size

	size (nm)	PDI	ζ potential (mV)
Pt@NP - 0 days	75 \pm 1	0.15 \pm 0.02	-32 ± 2
Pt@NP - 6 days	81 \pm 3	0.22 \pm 0.02	-36 ± 2

in size and PDI. The ζ potential, however, increased 10 to 15 mV on average owing to the additional positive charge from arginine in the peptide.

To prepare for the animal studies, we evaluated the stability of the NP constructs. Daily dosing would have demanded daily synthesis if the stability were low. Storage of the new constructs for up to six days at 4 $^{\circ}\text{C}$ in water did not change the Pt concentration, as determined by AAS after filtration, the size, or the ζ potential (Table 2). These results indicated that the constructs remain intact during this time period and under the conditions employed.

Integrin Expression. Expression of the $\alpha_v\beta_3$ integrin was quantified by flow cytometry using the FITC-conjugated mouse anti-human integrin $\alpha_v\beta_3$ monoclonal antibody MAB1976F. Expression levels were determined in three different cell lines of breast and prostate

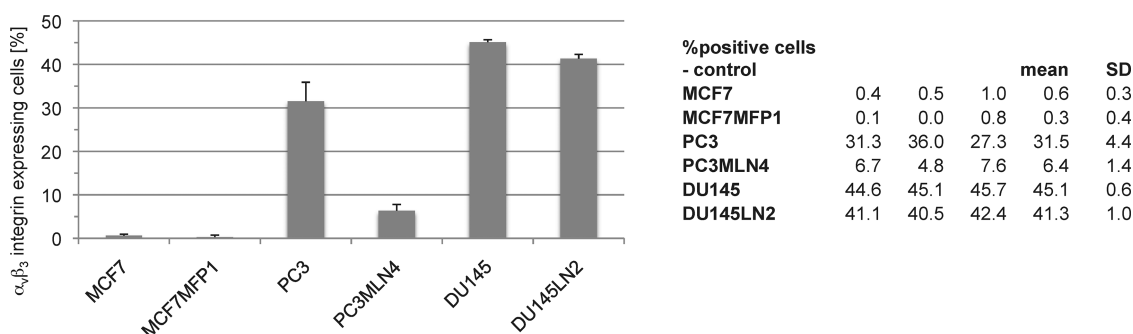


Figure 2. $\alpha_v\beta_3$ integrin expression was determined with a FITC-labeled antibody and analyzed by flow cytometry. The bars represent averages from three independent experiments (values obtained from non-labeled cells were subtracted, cf. Supporting Information Figure S2 for representative raw data histograms).

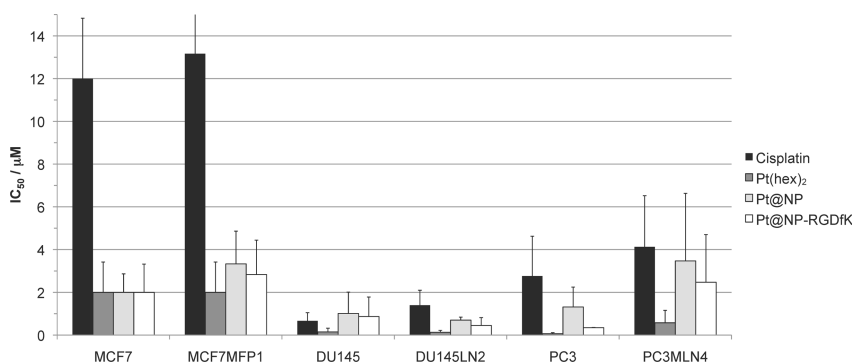


Figure 3. IC_{50} values – *in vitro* cytotoxicity against breast and prostate cancer cell lines. Averages and standard deviations from two to four experiments. Representative kill curves can be found in the Supporting Information Figure S4.

tumor origin (MCF7, PC3, DU145) and their metastatic counterparts (MCF7MFP1, PC3MLN4, DU145LN2) (Figure 2). Since many human tumor cell lines do not metastasize in nude mice as they do in their primary human location, we created metastatic cell lines by cycling *in vivo*. The cells were obtained by consecutive serial orthotopic implantation, where the letters in the cell line names stand for the site of recovery (LN = lymph nodes, MFP = mammary fat pad, M = liver metastases), and the numbers represent the number of cycles.

The $\alpha_v\beta_3$ integrin was expressed in high levels in PC3 cells (32%) and DU145 cells (45%). MCF-7 cells, however, lacked significant expression of $\alpha_v\beta_3$. These results are in accord with literature reported values (39 and 46%, respectively, for PC3 and DU145).^{42–45} The $\alpha_v\beta_3$ integrin levels of cycled cells were similar to those of the parental cell lines except for PC3 cell lines, where the expression levels of the cycled cells were lower.

Immunofluorescence. Once internalized by cells, Pt@NP-RGDfK is presumed to release Pt(hex)₂, which can be reduced to cisplatin and induce apoptosis by forming DNA adducts. The presence of Pt-1,2-d(GpG) intrastrand cross-links, the principal DNA adduct formed by cisplatin, in PC3MLN4 cells was confirmed by a monoclonal adduct-specific antibody (cf. Supporting Information Figure S3). As a positive control, cisplatin was used, and a negative control did not contain any Pt compound.

Cytotoxicity Studies. The $\alpha_v\beta_3$ integrins on the surfaces of breast and prostate cancer cells and their metastatic counterparts were targeted *in vitro* with the new Pt@NP-RGDfK constructs. Cell viability was assessed by the MTT assay (3-(4,5-dimethylthiazol-2-yl)-2,5-diphenyltetrazolium bromide) in monolayer cell culture. For comparison, cisplatin, Pt(hex)₂, and Pt@NP were also tested (Figure 3).

Cisplatin displays IC_{50} values on the order of magnitude of those in the literature, $\sim 2.8 \mu\text{M}$ for PC3, $\sim 0.7 \mu\text{M}$ for DU145, and $\sim 12 \mu\text{M}$ for MCF7 cells. Reported values using slightly different MTT protocols are $\sim 1.0 \mu\text{M}$ for PC3, $\sim 1.7 \mu\text{M}$ for DU145,⁴⁶ and $\sim 5 \mu\text{M}$ for MCF7.⁴⁷ The Pt(IV) compound, Pt(hex)₂, was more cytotoxic in all cell lines tested compared to the Pt(II) parental compound, cisplatin. As recently reported, the high lipophilicity of a Pt(IV) complex contributes to its increased cell killing ability.⁴⁸

The NP constructs were more active than cisplatin in all cancer cell lines. This result represents an improvement over the small molecule RGD–Pt(IV) construct that we previously reported, for which there was no increase in cytotoxicity compared to cisplatin.¹⁶ Protection of the Pt prodrug by the NP may give rise to the improved cytotoxicity. Our construct is more effective than a similar RGD-linked nanoscale coordination polymer used for the delivery of Pt(IV) complex prodrug.³⁴ For example, in MCF7 cells, only a 1.2-fold

improvement in cytotoxicity was observed for the nanoscale coordination polymer compared to cisplatin,³⁴ whereas we observed an increase in cytotoxicity by factor 6 by encapsulation of the Pt(IV) complex.

The cytotoxicity of Pt@NP-RGDfK is not supposed to emanate from the polymer or the RGD-targeting moiety of the NP construct. This expectation can be supported by a simple calculation. For 1% drug loading, a concentration of 1 μM Pt (the IC_{50} for DU145 cells) corresponds to 530 ng/mL Pt(IV) complex and thus 53 $\mu\text{g}/\text{mL}$ polymer. This value is still 40 times less than the IC_{50} obtained for the NP constructs without Pt encapsulated ($\text{IC}_{50}(\text{NP}) > 2 \text{ mg}/\text{mL}$, $\text{IC}_{50}(\text{NP-RGDfK}) > 2 \text{ mg}/\text{mL}$). In addition, the c(RGDfK) peptide alone is non-cytotoxic ($\text{IC}_{50} > 100 \mu\text{M}$, corresponding to 60 $\mu\text{g}/\text{mL}$). The latter value is 120-fold the peptide content presumed for the above mentioned IC_{50} for DU145 cells (1% w-peptide/w-polymer corresponds to 0.53 $\mu\text{g}/\text{mL}$ of c(RGDfK)).

The cytotoxicity of Pt@NP-RGDfK is superior to that of Pt@NP in the $\alpha_v\beta_3$ integrin positive cell lines PC3 and DU145, whereas in $\alpha_v\beta_3$ -negative MCF7 cells no obvious enhancement was observed. The result indicates that, when attached to the NP surface, the c(RGDfK) peptides successfully target $\alpha_v\beta_3$ integrins. This targeting effect, however, is small. The average IC_{50} values from several experiments, presented in Figure 3, as well as representative dose–response curves (Supporting Information Figure S4), attest to the relatively minor effect of the RGD peptide on the cytotoxicity.

There are two possible explanations for the enhancement of cytotoxic activity of Pt@NP and Pt@NP-RGDfK with respect to cisplatin.⁴⁹ First, NPs can absorb onto the cell membrane, leading to an increase in drug concentration near the cell surface, thus generating a concentration gradient that favors drug influx into the cell. Second, tumor cells, which often exhibit enhanced endocytotic activity, can also directly internalize the NPs, allowing the drug to be released into the interior of the cells, thus contributing to an increase of the drug concentration near its site of action. The low IC_{50} values for Pt@NP-RGDfK in $\alpha_v\beta_3$ integrin-positive cells also suggest that receptor-mediated endocytosis due to RGD binding to integrins may play a role.⁵⁰

Breast Cancer Xenograft. Factors influencing the uptake of RGD-functionalized NPs *in vivo* are the expression of $\alpha_v\beta_3$ integrins, not only on tumor cells but also on tumor vasculature. Thus, after having targeted these proteins on the surface of cancer cells (*in vitro*), we sought to explore the targeting properties *in vivo* in a breast cancer xenograft model based on MCF7 cells. Since MCF7 cells poorly express $\alpha_v\beta_3$ integrins (Figure 2), any observed effect on tumor growth can instead be attributed to targeting of endothelial cells of the angiogenic vasculature. Highly metastatic and tumorigenic breast carcinoma cells MCF7MFP1 were mixed with Matrigel and injected orthotopically into the mammary fat pad of 8-week-old female nude mice

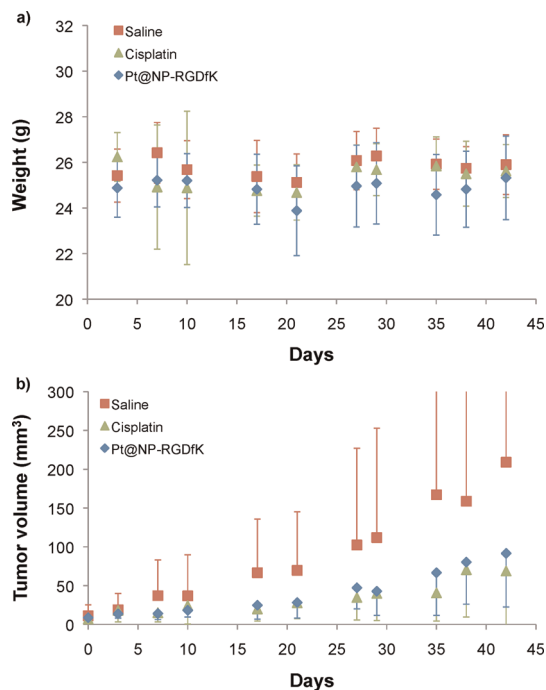


Figure 4. (a) Effects of cisplatin and Pt@NP-RGDfK on body weight of mice bearing MCF7MFP1 xenograft. Body weight was measured at the indicated time points. (b) Effects of cisplatin and Pt@NP-RGDfK on growth of MCF7MFP1 breast cancer xenografts. A dose of 0.8 mg/kg (with respect to Pt) or saline was administered intravenously, and the tumor size was measured at the indicated time points. Two mice (one in the saline, one in the cisplatin group) were disregarded for the evaluation since the tumor volume did not change within the time course.

($n = 15$). Slow-release pellets of 17 β -estradiol tablets were implanted subcutaneously on the dorsum of each mouse to ensure survival of the estrogen-dependent human breast tumor cells. After the tumor reached 1–2 mm in diameter, a value concurrent with the angiogenic switch, the mice were randomized into three groups and treated over six weeks by administering saline as a control, cisplatin, and Pt@NP-RGDfK every fourth day by intravenous injection at 0.8 mg/kg. No loss of body weight was observed in any group (Figure 4a). Over the course of six weeks, the average tumor volume increased from 8 to 209 mm^3 for the saline group, 69 mm^3 for the cisplatin group, and 92 mm^3 for the group treated with the NP construct Pt@NP-RGDfK (Figure 4b). These values correspond to tumor growth inhibitions (T/C) of 67% for cisplatin and 56% for the NPs. The analysis of variance by two-way ANOVA (with repeated measures on one factor) indicated that the difference among these Pt-treated groups was not significant ($P \gg 0.05$). Due to the targeting (passive and active) and the protecting environment for the Pt complex, we expected the NP system, however, to show better inhibition of tumor growth in comparison to cisplatin. It should be taken into account that the tumor can be sensitized directly by estrogen.⁵¹ Estrogen that was given for developing the tumors might have caused an enhanced response

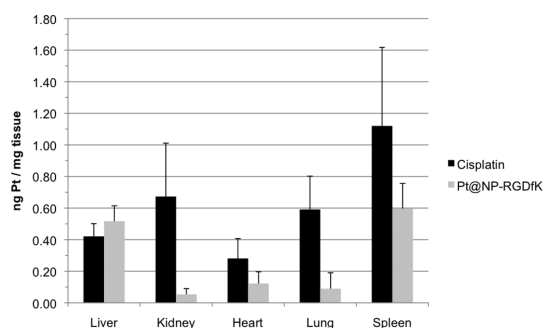


Figure 5. Distribution of Pt in mouse organs at 0.8 mg/kg dose cisplatin and Pt@NP-RGDfK (average and standard deviation for 5 mice/group).

to cisplatin, rendering growth inhibition results for cisplatin and the NP construct similar.

Next, the biodistribution of the Pt@NP-RGDfK was investigated. Organ samples were dissolved in nitric acid and hydrogen peroxide and subjected to AAS analysis for Pt determination.⁵² Figure 5 shows the results. Platinum accumulation in the liver was comparable for cisplatin and Pt@NP-RGDfK, whereas lower Pt uptake in the heart, kidney, spleen, and lung was observed for the NP system. The low impact on the latter organs has also been observed in a similar NP system comprising RNA aptamers instead of peptides as targeting moieties.²⁹

The Pt content in the kidney was lower by a factor of 10 for the NP construct than for cisplatin. This result is significant because a dose-limiting side effect of cisplatin is nephrotoxicity. Owing to possible filtration through liver and kidney excretion, particle size is a key factor. Intuitively, smaller nanoparticles enter cells more easily than larger nanoparticles, whereas the larger particles favorably target the tumor due to enhanced permeability and impaired lymphatic drainage (EPR effect). Polymeric NPs in the size range of 100–200 nm have the highest potential for long-time circulation because they are big enough to avoid uptake in the liver and rapid renal clearance²⁵ but

small enough to avoid filtering in the spleen.⁵³ NPs of a size of up to 100–200 nm can be taken up by cells *via* receptor-mediated endocytosis,⁵⁴ whereas the best EPR effect for a rigid particle is achieved for sizes <400 nm.²⁵ Particles with an average size of ~100 nm thus fulfill both restrictions and at the same time ensure good drug load and controlled release. Our nanoparticle system, exhibiting sizes of 75–140 nm, might therefore provide a more favorable biodistribution compared to that of cisplatin. Other biophysical properties like charge, surface hydrophilicity, and density of ligands on the surface of a NP can, however, also impact the biodistribution. These parameters are difficult to evaluate in the present study.^{55,56}

CONCLUSION

A polymeric NP system comprising an encapsulated Pt(IV) prodrug and cyclic RGD peptides as integrin-targeting moieties has been developed for anticancer therapy. The constructs were fully characterized and subjected to *in vitro* and *in vivo* tests for targeting $\alpha_v\beta_3$ integrins on cancer cells and epithelial cells of tumor vasculature, respectively. NPs inhibited growth of breast and prostate carcinoma cells *in vitro* at micromolar concentrations, a significant improvement over the parental drug cisplatin. *In vivo*, the constructs as well as cisplatin inhibited tumor growth of a human breast carcinoma xenografted in nude mice at a 0.8 mg/kg dose, and the NPs possibly exhibited reduced nephrotoxicity when compared to cisplatin as derived from Pt accumulation data. Because of the passive and active targeting of the NP system and protection of the cisplatin precursor [Pt(IV)], the NP is expected to show better inhibition of tumor growth in comparison to cisplatin itself. Both, however, showed similar tumor growth inhibition of ~60%. Considering the better biodistribution data for the NP system, dose–response studies might help to optimize its tumor growth-inhibition effect.

EXPERIMENTAL SECTION

Methods and Materials. Glycine buffer (Sørensen's glycine buffer) was prepared from 0.1 M glycine and 0.1 M NaCl adjusted to pH 10.5 with 1 M NaOH. MTT [3-(4,5-dimethylthiazol-2-yl)-2,5-diphenyltetrazolium bromide] solution was prepared at a concentration of 5 mg/mL in PBS, sonicated, and filter-sterilized (0.2 μ m). Concentrated solutions of cisplatin and Pt(hex)₂ were prepared by dissolving the compounds in PBS and dimethyl sulfoxide, respectively, followed by passage through a 0.2 μ m PTFE filter. The solutions were aliquotted for single use and stored at –20 °C for not longer than three months. Dilutions for *in vitro* tests were made with the respective medium. The Pt content of Pt stock solutions, Pt@NP suspensions, and organs of Pt-treated mice was determined by flameless AAS on a Perkin-Elmer AAnalyst 600 instrument.

Synthesis of Nanoparticles NP, Pt@NP, NP-RGDfK, and Pt@NP-RGDfK.

Nanoparticles were prepared using the nanoprecipitation method as reported previously.^{36,37} Briefly, the copolymer PLGA-PEG and Pt(hex)₂ were dissolved in acetonitrile at a final concentration of 5 mg/mL polymer and 30–50% w/w complex with respect to the polymer. The resulting solution was added to a 10-fold higher volume of Milli-Q water and stirred for up to 4 h. Alternatively, an Ultra-Turrax dispersing tool (T25 basic) at velocities of 6.5, 9.5, 13.5, 17.5, 21.5, and 24 k·min^{–1} was used. The NP suspension was filtered through filter paper and washed three times in Amicon centrifugal filter units MWCO 100 kDa at 3000 rpm and 4 °C. Alternatively, the ultrafiltration was carried out in a stirred ultrafiltration cell 8400 (Millipore, Billerica, MA, USA) using a XM50 membrane (76 mm) at 4 °C. Subsequently, the concentrated suspension was filtered through a 0.45 μ m filter.

A NP suspension (150 μL , 10 mg/mL) was treated with 400 mM EDC (1-ethyl-3-[3-dimethylaminopropyl]carbodiimide hydrochloride) and 100 mM NHS (*N*-hydroxysuccinimide) in water for 15 min at room temperature with agitation to give the corresponding PLGA-PEG-NHS ester. The activated NPs were washed twice using the Amicon centrifugal filter units to remove unreacted EDC and NHS. Conjugation to c(RGDfK) (Peptides International, Louisville, KY, USA) was performed by reacting 1.1% w/w peptide with respect to the polymer weight in water and agitating for 2 h at room temperature. The resulting NPs were washed three times with water with Amicon centrifugal units and resuspended in water for storage.

Similarly, a Pt-free construct (NP) and a Pt-free but RGD-conjugated construct (NP-RGDfK) were synthesized, omitting the Pt(hex)₂ solution during the nanoprecipitation step.

Arginine Determination. The peptide content of the nanoparticles was determined by measuring the arginine content as described previously.⁴¹ Briefly, 50 μL samples were mixed with 150 μL of 9,10-phenanthrenequinone reagent (150 μM in ethanol) and 25 μL of 2 N NaOH. Following a 3 h incubation at 60 °C, 200 μL of each sample was transferred to a disposable fluorescence PMMA (poly(methyl methacrylate)) cuvette and mixed with 200 μL of 1.2 N HCl. Fluorescence of the reaction product was allowed to develop for 1 h in the dark at room temperature and then measured at excitation/emission wavelengths of 312 nm/340–570 nm (maximum 395 nm) with a slitwidth of 0.8 mm on a Quanta Master 4 L-format scanning spectrofluorimeter (Photon Technology International, Birmingham, NJ). c(RGDfK) from 0 to 20 μg was used to test the linearity of the fluorescence signal (Supporting Information Figure S1).

Scanning Electron Microscopy (SEM). Samples for SEM were prepared by dropping a NP suspension onto a polished silicon wafer. Scanning electron microscopy images were obtained with a JEOL JSM6700F electron microscope operated at 10 kV.

Dynamic Light Scattering (DLS). DLS for size determination and ζ potential measurements was performed on a Malvern Zetasizer Nano ZS90 instrument (Malvern Instruments, Malvern, UK).

Cell Culture. Cells were cultured in DMEM (Dulbecco's Modified Eagle Medium) (MCF7 and MCF7MFP1) or RPMI-1640 (DU145, DU145LN2, PC3, PC3MLN4) containing 4.5 g/L glucose and L-glutamine, no sodium pyruvate, 10% FBS, 100 units/mL penicillin, and 100 $\mu\text{g}/\text{mL}$ streptomycin (all from Cellgro, Manassas, VA, USA) at 37 °C in a humidified atmosphere at 5% CO₂.

Flow Cytometry. Cells were harvested from T-25 flasks by trypsin treatment, counted, and washed with ice-cold PBS/5% FBS/0.1%Na₃. A total of 500 000 cells was incubated with or without a 1:100 dilution of FITC-conjugated mouse anti-human integrin $\alpha_v\beta_3$ antibody MAB1976F (1 μg , Millipore, Temecula, CA, USA) in 100 μL PBS/5% FBS/0.1%Na₃ for 1 h on ice. The cells were washed three times with 0.5 mL of ice-cold PBS/5% FBS/0.1%Na₃, resuspended in 500 μL of the same mixture, and then subjected to flow cytometric analysis on a BD FACScan system.

Immunofluorescence. The detection of Pt-1,2-d(GpG) cross-links on the DNA of PC3MLN4 cells was achieved by following a procedure similar to one previously reported using an adduct-specific antibody.⁵⁷

PC3MLN4 cells were plated in 6-well plates, grown for 1–3 days, and incubated for 16 h with 1 μM cisplatin, 1 μM Pt@NP-RGDfK, or medium only, respectively. The cells were trypsinized, washed with medium and two times PBS, and resuspended in 2.5% hydroxyethyl starch diluted with PBS (Hetastarch, Hospira, Lake Forest, IL, USA) at a concentration of 10⁶/mL. Drops of 10 μL were placed onto ImmunoSelect slides (Squarix, Marl, Germany) containing 10 000 cells, air-dried, circled with an ImmEdge Hydrophobic Barrier Pen (Vector Laboratories, Burlingame, CA, USA), and stored at –20 °C until analysis.

Cell fixation was carried out for 45 min in methanol at –20 °C. After rehydration for 5 min with PBS, an alkali denaturation step followed (precooled 40% MeOH with 70 mM NaOH/140 mM NaCl) for 5 min at 0 °C. The cells were washed two times with PBS for 5 min. Cellular proteins were digested with pepsin (freshly prepared solution of 30 $\mu\text{g}/\text{mL}$ in PBS/HCl pH 6) and proteinase K (1 mg/mL stock in buffer containing 20 mM Tris base, 2 mM CaCl₂, pH 7.5, stored at –20 °C). A 100 μL drop of

prewarmed pepsin per spot was added and incubated for 10 min at 37 °C in a moist chamber, and the spots were then washed two times with PBS. A drop of 100 μL 6 $\mu\text{g}/\text{mL}$ prewarmed proteinase K was incubated the same way, then washed in PBS/glycine (0.2%) at room temperature for 10 min. Blocking was done with PBS–5% milk powder for 30 min at room temperature. The cells were then incubated with 0.2 $\mu\text{g}/\text{mL}$ anti-(Pt-1,2-d(GpG)) antibody MAB RC-18 in PBS–1% milk powder at 37 °C for 3 h, and washed two times with PBS for 5 min. After blocking with PBS–5% milk powder for 30 min at room temperature, immunostaining with the secondary antibody anti-rat-IgG-FITC (from rabbit, F1763, Sigma) was performed with a 1:320 dilution for 1 h at 37 °C. Excess antibody was removed by three washes with PBS for 5 min. Nuclei were stained with 1.4 $\mu\text{g}/\text{mL}$ Hoechst H33258 for 10 min at room temperature, followed by a wash with PBS for 10 min. The slides were mounted with antifading solution (0.05 g *n*-propyl gallate, 1 mL Tris-HCl 1 M pH 8.0, 9 mL of glycerol). The fluorescence images were taken with a Zeiss Axiovert 200 M inverted epifluorescence microscope equipped with an EM-CCD digital camera (Hamamatsu).

Cytotoxicity Tests⁵⁸. The cells were plated in flat-bottomed 96-well plates starting with column 2 and ending with column 11 (1000 cells/well for prostate cancer cells, 2000 cells/well for slower growing breast cancer cells). The plates were incubated at 37 °C for 2–3 days such that cells were in the exponential phase of growth for drug addition. A serial 4-fold dilution of the compound to be tested in growth medium was prepared to give eight concentrations of 2 mL each (1.5 mL medium + 0.5 mL drug dilution, 0.006–100 μM for Pt or peptide, 0.12–2000 $\mu\text{g}/\text{mL}$ for polymeric material). The medium was removed from all wells, and the drug was added in the several dilutions in fresh growth medium. The plates were incubated for 72 h. At the end of the drug-exposure period, the medium was removed and the plates were treated with 200 μL of MTT solution (stock 1:5 in medium). The plates were incubated for 4 h in a humidified atmosphere at 37 °C. The medium was removed from the wells, and the purple MTT-formazan crystals were dissolved by addition of 200 μL of DMSO/glycine buffer pH 10.5 (8:1). Since the absorption spectrum of MTT-formazan is pH-dependent, and the pH varies with the cell density in the well, the pH in all wells was adjusted to 10.5 where the spectrum shows only a single peak at 570 nm.⁵⁸ The absorbance was measured at this maximum on a SynergyHT platereader (BioTek, Winooski, VT, USA), and the mean absorbance reading from the wells without drug was used as the control (100% viability). IC₅₀ values were determined by interpolation of the resulting curves.

Animal Studies. Female nude mice (8 weeks old) were obtained from Charles River Laboratories (Wilmington, MA, USA) and were allowed to acclimate for at least 5 days. They were housed under aseptic conditions and given autoclaved rodent diet and sterile water *ad libitum*.

Metastatic breast cancer cells (MCF7MFP1) were grown to 80% confluence in 150 mm tissue culture dishes. After harvesting, cells were suspended in Hank's Balanced Salt Solution (HBSS) and mixed 1:1 (v:v) with Matrigel (BD, Sparks, MD, USA) at 4 °C to a final concentration of 2.5 \times 10⁷ cells/mL. Mice (*n* = 15) were anesthetized with isoflurane, and a small incision was made near the fourth inguinal gland. The skin was retracted to expose the mammary fat pad, and a 40 μL tumor cell suspension containing 10⁶ cells in a 1 mL disposable syringe was injected into the fat pad beneath the nipple using a 30 G needle and a calibrated push-button-controlled dispensing device. 17 β -Estradiol tablets (slow release over 60 days, IRA, Sarasota, FL, USA) were implanted subcutaneously on the dorsum. All incisions were closed with wound clips. After the tumor reached ~2 mm in diameter, 14 days after transplantation, the animals were randomized into three groups.

The mice were treated over six weeks by administering saline as a control, cisplatin, and targeted Pt-encapsulated NPs every fourth day intravenously in 100 μL at a dose of 0.8 mg/kg. The NPs, Pt@NP-RGDfK, were reconstituted in 1 \times PBS and filtered 0.2 μm freshly before the injection. Tumor growth and body weight were monitored and recorded twice weekly. Tumors were measured by determining the length and width

with calipers. Tumor volume was calculated using the following formula: $TV = (L \times W^2)/2$, with W being smaller than L . The percentage tumor growth inhibition was calculated as follows: $100(1 - T/C)$, where T is the mean tumor size for a drug-treated group on a given day and C is the mean tumor size for the control group. Mice were sacrificed by CO_2 inhalation when their tumors reached the 300 mm^3 endpoint value or after 7 weeks.

All animal procedures were approved by the Children's Hospital Boston Animal Care and Use Committee (IACUC) and the Committee on Animal Care at MIT.

Analysis of Pt Content in Mouse Organs. Organ samples of all 15 mice were prepared for analysis of their Pt content by AA similar to a procedure published previously.⁵² A 200 mg tissue sample was incubated in $500 \mu\text{L}$ of concentrated nitric acid overnight at room temperature. The sample was boiled for 3 min, cooled to room temperature, and $500 \mu\text{L}$ of 30% hydrogen peroxide was added. After boiling for 5 min, the volume was adjusted to 1 mL with Milli-Q water. The furnace parameters for the AA measurement were as reported before⁵² but adjusted to our instrumental setting: dry 150°C , ramp 10 s, hold 30 s — dry 350°C , ramp 10 s, hold 30 s — char 1300°C , ramp 10 s, hold 50 s — atomize 2200°C , ramp 0 s, hold 5 s — clean 2600°C , ramp 1 s, hold 3 s; for all steps (except the atomization with 0 mL/min), the flow rate was 250 mL/min.

Conflict of Interest: The authors declare the following competing financial interest(s): Dr. Farokhzad declares a financial interest in BIND Biosciences and Selecta Biosciences. Drs. Lippard and Farokhzad declare a financial interest in Blend Therapeutics.

Acknowledgment. This work was supported by Grant CA034992 (to S.J.L.) and CA119349 (to O.C.F.) from the National Cancer Institute and by Grant EB003647 (to O.C.F.) from the National Institute of Biomedical Imaging and Bioengineering as well as by the Koch-Prostate Cancer Foundation Award in Nanotherapeutics (to O.C.F.). The monoclonal Pt-1,2-d(GpG) adduct-specific antibody R-C18 was kindly provided by Prof. Jürgen Thomale (University of Duisburg-Essen, Germany). N.G. and C.M. thank DAAD (German Academic Exchange Service) for their fellowships. We thank Carmen M. Barnés for helpful discussions.

Supporting Information Available: Calibration curve arginine determination, flow cytometry $\alpha_v\beta_3$ integrin expression, immunofluorescence Pt-1,2-d(GpG) cross-links, kill curves. This material is available free of charge via the Internet at <http://pubs.acs.org>.

REFERENCES AND NOTES

1. *Cisplatin. Chemistry and Biochemistry of a Leading Anti-cancer Drug*; Lippert, B., Ed.; Wiley-VCH/Helvetica Chimica Acta: Zürich, 1999.
2. Ott, I.; Gust, R. Preclinical and Clinical Studies on the Use of Platinum Complexes for Breast Cancer Treatment. *Anti-Cancer Agents Med. Chem.* **2007**, *7*, 95–110.
3. Ivanov, A. I.; Christodoulou, J.; Parkinson, J. A.; Barnham, K. J.; Tucker, A.; Woodrow, J.; Sadler, P. J. Cisplatin Binding Sites on Human Albumin. *J. Biol. Chem.* **1998**, *273*, 14721–14730.
4. Graf, N.; Lippard, S. J. Redox Activation of Metal-Based Prodrugs as a Strategy for Drug Delivery. *Adv. Drug Delivery Rev.* **2012**, DOI: 10.1016/j.addr.2012.01.007.
5. Hall, M. D.; Hambley, T. W. Platinum(IV) Antitumor Compounds: Their Bioinorganic Chemistry. *Coord. Chem. Rev.* **2002**, *232*, 49–67.
6. Kamaly, N.; Xiao, Z.; Valencia, P. M.; Radovic-Moreno, A. F.; Farokhzad, O. C. Targeted Polymeric Therapeutic Nanoparticles: Design, Development and Clinical Translation. *Chem. Soc. Rev.* **2012**, *41*, 2971–3010.
7. Eliceiri, B. P.; Cheres, D. A. Adhesion Events in Angiogenesis. *Curr. Opin. Cell Biol.* **2001**, *13*, 563–568.
8. Felding-Habermann, B.; O'Toole, T. E.; Smith, J. W.; Fransvea, E.; Ruggeri, Z. M.; Ginsberg, M. H.; Hughes, P. E.; Pampori, N.; Shattil, S. J.; Saven, A.; et al. Integrin Activation Controls Metastasis in Human Breast Cancer. *Proc. Natl. Acad. Sci. U.S.A.* **2001**, *98*, 1853–1858.
9. Tucker, G. C. Integrins: Molecular Targets in Cancer Therapy. *Curr. Oncol. Rep.* **2006**, *8*, 96–103.
10. Arap, W.; Pasqualini, R.; Ruoslahti, E. Cancer Treatment by Targeted Drug Delivery to Tumor Vasculature in a Mouse Model. *Science* **1998**, *279*, 377–380.
11. Pasqualini, R.; Koivunen, E.; Ruoslahti, E. α_v Integrins as Receptors for Tumor Targeting by Circulating Ligands. *Nat. Biotechnol.* **1997**, *15*, 542–546.
12. Haubner, R.; Wester, H.-J.; Reuning, U.; Senekowitsch-Schmidtke, R.; Diefenbach, B.; Kessler, H.; Stöcklin, G.; Schwaiger, M. Radiolabeled $\alpha_v\beta_3$ Integrin Antagonists: A New Class of Tracers for Tumor Targeting. *J. Nucl. Med.* **1999**, *40*, 1061–1071.
13. Janssen, M. L.; Oyen, W. J.; Dijkgraaf, I.; Massuger, L. F.; Frielink, C.; Edwards, D. S.; Rajopadhye, M.; Boonstra, H.; Corstens, F. H.; Boerman, O. C. Tumor Targeting with Radiolabeled $\alpha_v\beta_3$ Integrin Binding Peptides in a Nude Mouse Model. *Cancer Res.* **2002**, *62*, 6146–6151.
14. Liu, Z.; Yan, Y.; Liu, S.; Wang, F.; Chen, X. ^{18}F , ^{64}Cu , and ^{68}Ga Labeled RGD-Bombesin Heterodimeric Peptides for PET Imaging of Breast Cancer. *Bioconjugate Chem.* **2009**, *20*, 1016–1025.
15. Schottelius, M.; Wester, H.-J. Molecular Imaging Targeting Peptide Receptors. *Methods* **2009**, *48*, 161–177.
16. Mukhopadhyay, S.; Barnés, C. M.; Haskel, A.; Short, S. M.; Barnes, K. R.; Lippard, S. J. Conjugated Platinum(IV)-Peptide Complexes for Targeting Angiogenic Tumor Vasculature. *Bioconjugate Chem.* **2008**, *19*, 39–49.
17. Bibby, D. C.; Talmadge, J. E.; Dalal, M. K.; Kurz, S. G.; Chytil, K. M.; Barry, S. E.; Shand, D. G.; Steiert, M. Pharmacokinetics and Biodistribution of RGD-Targeted Doxorubicin-Loaded Nanoparticles in Tumor-Bearing Mice. *Int. J. Pharm.* **2005**, *293*, 281–290.
18. Cai, W.; Shin, D.-W.; Chen, K.; Gheysens, O.; Cao, Q.; Wang, S. X.; Gambhir, S. S.; Chen, X. Peptide-Labeled Near-Infrared Quantum Dots for Imaging Tumor Vasculature in Living Subjects. *Nano Lett.* **2006**, *6*, 669–676.
19. Desgrosellier, J. S.; Cheres, D. A. Integrins in Cancer: Biological Implications and Therapeutic Opportunities. *Nat. Rev. Cancer* **2010**, *10*, 9–22.
20. Lee, H.-Y.; Li, Z.; Chen, K.; Hsu, A. R.; Xu, C.; Xie, J.; Sun, S.; Chen, X. PET/MRI Dual-Modality Tumor Imaging Using Arginine-Glycine-Aspartic (RGD)-Conjugated Radiolabeled Iron Oxide Nanoparticles. *J. Nucl. Med.* **2008**, *49*, 1371–1379.
21. Lu, J.; Shi, M.; Shoichet, M. S. Click Chemistry Functionalized Polymeric Nanoparticles Target Corneal Epithelial Cells through RGD-Cell Surface Receptors. *Bioconjugate Chem.* **2009**, *20*, 87–94.
22. Montet, X.; Funovics, M.; Montet-Abou, K.; Weissleder, R.; Josephson, L. Multivalent Effects of RGD Peptides Obtained by Nanoparticle Display. *J. Med. Chem.* **2006**, *49*, 6087–6093.
23. Zako, T.; Nagata, H.; Terada, N.; Utsumi, A.; Sakono, M.; Yohda, M.; Ueda, H.; Soga, K.; Maeda, M. Cyclic RGD Peptide-Labeled Upconversion Nanophosphors for Tumor Cell-Targeted Imaging. *Biochem. Biophys. Res. Commun.* **2009**, *381*, 54–58.
24. Zhang, N.; Chittasupho, C.; Duangrat, C.; Siahaan, T. J.; Berkland, C. PLGA Nanoparticle-Peptide Conjugate Effectively Targets Intercellular Cell-Adhesion Molecule-1. *Bioconjugate Chem.* **2008**, *19*, 145–152.
25. Alexis, F.; Pridgen, E.; Molnar, L. K.; Farokhzad, O. C. Factors Affecting the Clearance and Biodistribution of Polymeric Nanoparticles. *Mol. Pharm.* **2008**, *5*, 505–515.
26. Temming, K.; Schifferers, R. M.; Molema, G.; Kok, R. J. RGD-Based Strategies for Selective Delivery of Therapeutics and Imaging Agents to the Tumor Vasculature. *Drug Resist. Updates* **2005**, *8*, 381–402.
27. Peer, D.; Karp, J. M.; Hong, S.; Farokhzad, O. C.; Margalit, R.; Langer, R. Nanocarriers as an Emerging Platform for Cancer Therapy. *Nat. Nanotechnol.* **2007**, *2*, 751–760.

28. Matsumura, Y.; Maeda, H. A New Concept for Macromolecular Therapeutics in Cancer Chemotherapy: Mechanism of Tumorotropic Accumulation of Proteins and the Antitumor Agent Smancs. *Cancer Res.* **1986**, *46*, 6387–6392.
29. Dhar, S.; Kolishetti, N.; Lippard, S. J.; Farokhzad, O. C. Targeted Delivery of a Cisplatin Prodrug for Safer and More Effective Prostate Cancer Therapy *in Vivo*. *Proc. Natl. Acad. Sci. U.S.A.* **2011**, *108*, 1850–1855.
30. Haxton, K. J.; Burt, H. M. Polymeric Drug Delivery of Platinum-Based Anticancer Agents. *J. Pharm. Sci.* **2009**, *98*, 2299–2316.
31. Paraskar, A. S.; Soni, S.; Chin, K. T.; Chaudhuri, P.; Muto, K. W.; Berkowitz, J.; Handlogten, M. W.; Alves, N. J.; Bilgicer, B.; Dinulescu, D. M.; *et al.* Harnessing Structure-Activity Relationship To Engineer a Cisplatin Nanoparticle for Enhanced Antitumor Efficacy. *Proc. Natl. Acad. Sci. U.S.A.* **2010**, *107*, 12435–12440.
32. Xing, R.; Wang, X.; Zhang, C.; Zhang, Y.; Wang, Q.; Yang, Z.; Guo, Z. Characterization and Cellular Uptake of Platinum Anticancer Drugs Encapsulated in Apoferritin. *J. Inorg. Biochem.* **2009**, *103*, 1039–1044.
33. Aryal, S.; Hu, C.-M. J.; Zhang, L. Polymer-Cisplatin Conjugate Nanoparticles for Acid-Responsive Drug Delivery. *ACS Nano* **2010**, *4*, 251–258.
34. Rieter, W. J.; Pott, K. M.; Taylor, K. M. L.; Lin, W. Nanoscale Coordination Polymers for Platinum-Based Anticancer Drug Delivery. *J. Am. Chem. Soc.* **2008**, *130*, 11584–11585.
35. Harper, B. W.; Krause-Heuer, A. M.; Grant, M. P.; Manohar, M.; Garbutcheon-Singh, K. B.; Aldrich-Wright, J. R. Advances in Platinum Chemotherapeutics. *Chem. Eur. J.* **2010**, *16*, 7064–7077.
36. Dhar, S.; Gu, F. X.; Langer, R.; Farokhzad, O. C.; Lippard, S. J. Targeted Delivery of Cisplatin to Prostate Cancer Cells by Aptamer Functionalized Pt(IV) Prodrug-PLGA-PEG Nanoparticles. *Proc. Natl. Acad. Sci. U.S.A.* **2008**, *105*, 17356–17361.
37. Farokhzad, O. C.; Cheng, J.; Teply, B. A.; Sherifi, I.; Jon, S.; Kantoff, P. W.; Richie, J. P.; Langer, R. Targeted Nanoparticle-Aptamer Bioconjugates for Cancer Chemotherapy *in Vivo*. *Proc. Natl. Acad. Sci. U.S.A.* **2006**, *103*, 6315–6320.
38. Otsuka, H.; Nagasaki, Y.; Kataoka, K. PEGylated Nanoparticles for Biological and Pharmaceutical Applications. *Adv. Drug Delivery Rev.* **2003**, *55*, 403–419.
39. Langer, R. Drug Delivery and Targeting. *Nature* **1998**, *392* (Suppl), 5–10.
40. Wester, H.-J.; Kessler, H. Molecular Targeting with Peptides or Peptide-Polymer Conjugates: Just a Question of Size? *J. Nucl. Med.* **2005**, *46*, 1940–1945.
41. Schmitt, A.; Schmitt, J.; Münch, G.; Gasic-Milencovic, J. Characterization of Advanced Glycation End Products for Biochemical Studies: Side Chain Modifications and Fluorescence Characteristics. *Anal. Biochem.* **2005**, *338*, 201–215.
42. Borgman, M. P.; Ray, A.; Kolhatkar, R. B.; Sausville, E. A.; Burger, A. M.; Ghandehari, H. Targetable HPMA Copolymer-Aminohexylgeldanamycin Conjugates for Prostate Cancer Therapy. *Pharm. Res.* **2009**, *26*, 1407–1418.
43. Marelli, M. M.; Moretti, R. M.; Procacci, P.; Motta, M.; Limonta, P. Insulin-like Growth Factor-I Promotes Migration in Human Androgen-Independent Prostate Cancer Cells *via* the $\alpha_v\beta_3$ Integrin and PI3-K/Akt Signaling. *Int. J. Oncol.* **2006**, *28*, 723–730.
44. Cooper, C. R.; Chay, C. H.; Pienta, K. J. The Role of $\alpha_v\beta_3$ in Prostate Cancer Progression. *Neoplasia* **2002**, *4*, 191–194.
45. Wong, N. C.; Mueller, B. M.; Barbas, C. F.; Ruminiski, P.; Quaranta, V.; Lin, E. C. K.; Smith, J. W. α_v Integrins Mediate Adhesion and Migration of Breast Carcinoma Cell Lines. *Clin. Exp. Metastasis* **1998**, *16*, 50–61.
46. Wosikowski, K.; Lamphere, L.; Unteregger, G.; Jung, V.; Kaplan, F.; Xu, J. P.; Rattel, B.; Caligiuri, M. Preclinical Antitumor Activity of the Oral Platinum Analog Satraplatin. *Cancer Chemother. Pharmacol.* **2007**, *60*, 589–600.
47. Basma, H.; El-Refaey, H.; Sgagias, M. K.; Cowan, K. H.; Luo, X.; Cheng, P.-W. BCL-2 Antisense and Cisplatin Combination Treatment of MCF-7 Breast Cancer Cells with or without Functional p53. *J. Biomed. Sci.* **2005**, *12*, 999–1011.
48. Reithofer, M. R.; Bytzek, A. K.; Valiahdi, S. M.; Kowol, C. R.; Groessl, M.; Hartinger, C. G.; Jakupec, M. A.; Galanski, M.; Keppler, B. K. Tuning of Lipophilicity and Cytotoxic Potency by Structural Variation of Anticancer Platinum(IV) Complexes. *J. Inorg. Biochem.* **2011**, *105*, 46–51.
49. Fonseca, C.; Simões, S.; Gaspar, R. Paclitaxel-Loaded PLGA Nanoparticles: Preparation, Physicochemical Characterization and *in Vitro* Anti-tumoral Activity. *J. Controlled Release* **2002**, *83*, 273–286.
50. Oba, M.; Fukushima, S.; Kanayama, N.; Aoyagi, K.; Nishiyama, N.; Koyama, H.; Kataoka, K. Cyclic RGD Peptide-Conjugated Polyplex Micelles as a Targetable Gene Delivery System Directed to Cells Possessing $\alpha_v\beta_3$ and $\alpha_v\beta_5$ Integrins. *Bioconjugate Chem.* **2007**, *18*, 1415–1423.
51. He, Q.; Liang, C. H.; Lippard, S. J. Steroid Hormones Induce HMG1 Overexpression and Sensitize Breast Cancer Cells to Cisplatin and Carboplatin. *Proc. Natl. Acad. Sci. U.S.A.* **2000**, *97*, 5768–5772.
52. McGahan, M. C.; Tyczkowska, K. The Determination of Platinum in Biological Materials by Electrothermal Atomic-Absorption Spectroscopy. *Spectrochim. Acta B* **1987**, *42*, 665–668.
53. Petros, R. A.; DeSimone, J. M. Strategies in the Design of Nanoparticles for Therapeutic Applications. *Nat. Rev. Drug Discov.* **2010**, *9*, 615–627.
54. Win, K. Y.; Feng, S.-S. Effects of Particle Size and Surface Coating on Cellular Uptake of Polymeric Nanoparticles for Oral Delivery of Anticancer Drugs. *Biomaterials* **2005**, *26*, 2713–2722.
55. Farokhzad, O. C.; Langer, R. Impact of Nanotechnology on Drug Delivery. *ACS Nano* **2009**, *3*, 16–20.
56. Davis, M. E.; Chen, Z.; Shin, D. M. Nanoparticle Therapeutics: An Emerging Treatment Modality for Cancer. *Nat. Rev. Drug Discov.* **2008**, *7*, 771–782.
57. Dhar, S.; Liu, Z.; Thomale, J.; Dai, H.; Lippard, S. J. Targeted Single-Wall Carbon Nanotube-Mediated Pt(IV) Prodrug Delivery Using Folate as a Homing Device. *J. Am. Chem. Soc.* **2008**, *130*, 11467–11476.
58. Plumb, J. A. Cell Sensitivity Assays: The MTT Assay. In *Cytotoxic Drug Resistance Mechanisms*; Brown, R., Böger-Brown, U., Eds.; Methods in Molecular Medicine; Humana Press: New York, 1999; Vol. 28, pp 25–30.